Structure of the Transition State of Gating in the Acetylcholine Receptor Channel Pore: A Φ-Value Analysis†

Gisela D. Cymes, Claudio Grosman,* and Anthony Auerbach

Center for Single-Molecule Biophysics and Department of Physiology and Biophysics, State University of New York at Buffalo, Buffalo, New York 14214

Received October 1, 2001; Revised Manuscript Received January 22, 2002

ABSTRACT: The gating mechanism of the acetylcholine receptor channel (AChR) was investigated by using rate equilibrium linear free energy relationships (LFERs) to probe the transition state between the closed and open conformations. The properties of the transition state of gating in the second transmembrane segment (M2) of the δ subunit, one of the five homologous pore-lining segments, was measured on a residue-by-residue basis. Series of point mutations were engineered at individual positions of this domain, and the corresponding constructs were characterized electrophysiologically, at the single-channel level. Fully liganded AChR opening and closing rate constants were estimated, and Φ-values (which are a measure of the extent of the conformational change realized at the transition state) were calculated for each reaction series as the slope of the Brønsted relationship (log rate constant versus log equilibrium constant). Our results indicate that, at the transition state of gating, the extracellular half of δM2 partly resembles the open state (Φ-values between 0.24 and 0.38) while the intracellular half completely resembles the closed state (Φ-values between −0.18 and 0.03), with a break point near the middle of the M2 segment. This suggests that during gating the two halves of δM2 move asynchronously, with the rearrangement of the extracellular portion preceding (following) that of the intracellular part of δM2 during opening (closing). This particular sequence of molecular events indicates that the gating conformational change, which starts at the extracellular acetylcholine-binding sites (when opening), does not propagate exclusively along the primary sequence of the protein. In addition, our data are consistent with the δM2 segment bending or swiveling around its central residues during gating. We also elaborate on unsettled aspects of the analysis such as the accuracy of two-point LFERs, the physical interpretation of fractional Φ-values, and the existence of single versus parallel transition states for the gating reaction.

The acetylcholine receptor channel (AChR)[1] is a large (∼290 kDa) allosteric membrane protein that mediates synaptic transmission at the vertebrate neuromuscular junction. It consists of five homologous subunits ($\alpha_2\beta\delta\epsilon$ in adult muscle) that form a cation-selective pathway across the membrane. Each subunit is thought to contain four transmembrane segments (M1−M4), a structural feature shared with the other members of the nicotinoid receptor superfamily (which includes nicotinic, 5-HT_3, glycine, $GABA_A$, and $GABA_C$ receptors). The second membrane-spanning domain, M2, is of particular interest because it forms the pentameric α-helical bundle that contributes most of the pore lining (*1*−*5*).

Several lines of evidence suggest that the M2 segments are bent (*6*, *7*) or disordered (*7*, *8*) at their midpoints and that this discontinuity in the proposed α-helical structure could act as a molecular hinge or swivel during gating (*9*). It is well-known that some degree of conformational freedom is afforded by a break in the H-bond system that stabilizes an α-helix. Indeed, an interrupted network of hydrogen bonds was described in the vicinity of the central 9′ Leu (*10*, *11*).

Although the atomic resolution structures of the AChR in the closed and open states are still not known, opening must involve conformational changes in at least two domains: the transmitter binding sites, which switch from low to high agonist affinity, and the pore [∼45 Å away from the binding sites (*6*, *12*, *13*)], which switches from ion-impermeable to ion-permeable. The sequence of events that links these two end states (i.e., the gating mechanism) is also unknown, and for its elucidation, some knowledge about stable reaction intermediates is needed. Because gating of diliganded AChRs appears to be a one-step conformational change (*14*), the only intermediate conformation that is amenable to characterization is the transition state, that is, the transient conformation between the end states with the highest free energy.

Structural information about the transition state can be gained from the analysis of kinetic data in the framework of rate equilibrium linear free energy relationships [LFERs (*15*−*17*)]. The LFER formalism rationalizes the positive correlation frequently found between the forward rate constant of a one-step reaction and its equilibrium constant, when plotted on logarithmic axes [a "Brønsted plot" (*18*)]. For each reaction series (in our case, a number of AChR constructs differing only in the amino acid residue at a given position), the slope of this relationship (Φ) is an estimate of the structure of the receptor in the environment of the mutated

† This work was supported by grants from the American Heart Association (New York State Affiliate) to G.D.C. and C.G., the NIH (NS23513 and RR11111), and the Keck Foundation to A.A.

* To whom correspondence should be addressed. Tel: 716-829-2435. Fax: 716-829-2569. E-mail: grosman@buffalo.edu or grosman@life.uiuc.edu.

[1] Abbreviations: AChR, acetylcholine receptor channel; M2, second transmembrane segment; LFER, linear free energy relationship.

10.1021/bi011864f CCC: $22.00
Published on Web 04/06/2002

position, at the transition state. Φ usually ranges between 0 and 1, with a value of zero indicating a closed state-like structure and a value of 1 indicating an open state-like structure. We have previously obtained a low-resolution LFER snapshot of the AChR at the gating transition state (*17*). These results suggested the existence of a spatial gradient of Φ-values along the long axis of the receptor, which led to the conclusion that during the conformational change associated with opening the low-to-high affinity change at the transmitter-binding sites precedes the complete opening of the pore.

Here we present a high-resolution map of Φ-values in the M2 segment of the δ subunit of the muscle AChR, which illuminates the dynamics of gating of this important channel domain. Our results are consistent with the notion that the δM2 α-helix bends or swivels about its central residues during gating, with the conformational change of the extracellular half preceding the movement of the intracellular half upon opening. We also elaborate on three unsettled aspects of the analysis, namely, the accuracy of two-point LFERs, the physical interpretation of fractional Φ-values, and the existence of single versus parallel transition states for the gating reaction.

MATERIALS AND METHODS

Mutagenesis and Expression. cDNA clones corresponding to the α, β, δ, and ε subunits of the mouse muscle AChR were obtained as described in ref *19*. The α subunit had a Val-to-Ala background mutation in the M4 segment that has been shown not to affect channel gating (*20*). Site-directed mutations were engineered on the δ subunit using the QuikChange site-directed mutagenesis kit (Stratagene) protocol and confirmed by dideoxy sequencing. There was no rationale behind the choice of mutations. In practice, the idea of the LFER approach is to "move" the equilibrium constant of a reaction in small steps to an extent that is large enough to allow an unbiased estimate of the slope of a Brønsted plot. However, because the relationship between the structural features of M2 and the magnitude of the gating equilibrium constant is poorly understood, we could not anticipate which mutations would work best. Thus, the choice of mutations was largely random. Despite this lack of rationale, the linearity of the Brønsted plots (an absolute requirement for the application of the LFER approach) was conserved in all but one position.

Human embryonic kidney fibroblast cells (HEK 293) were transiently transfected using calcium phosphate precipitation. A total of 3.5 μg of cDNA per 35 mm culture dish in the ratio 2:1:1:1 (α:β:δ:ε) was applied to the cells for ~22 h, after which time the medium was changed. Electrophysiological recordings started ~24 h later.

Single-Channel Recordings. Recordings were performed in the cell-attached patch-clamp configuration (*21*) at ~22 °C. The bath and pipet solutions were Dulbecco's phosphate-buffered saline containing (mM) 137 NaCl, 0.9 $CaCl_2$, 2.7 KCl, 1.5 KH_2PO_4, 0.5 $MgCl_2$, and 8.1 Na_2HPO_4, pH 7.3. Patch pipets, pulled from borosilicate capillaries, were coated with Sylgard (Dow Corning Corp.) and fire-polished to a final resistance of 5−8 MΩ. The potential of the patch pipet was held at +70 mV which, in the cell-attached configuration, corresponds to an estimated membrane potential of ~−100 mV. Single-channel currents were recorded using an Axopatch 200A amplifier (Axon Instruments) at a 10 kHz bandwidth and were transferred directly into a Pentium III computer (dual processor, 550 MHz each) at a sampling frequency of 40 or 100 kHz, using a National Instruments PCI-MIO-14E-4 acquisition board.

Gating Kinetics. Gating of diliganded AChRs can be modeled as a single-step reaction:

$$CA_2 \underset{\alpha}{\overset{\beta}{\rightleftharpoons}} OA_2$$

where CA_2 is the diliganded closed receptor and OA_2 is the diliganded open receptor. Because in the presence of ACh the opening rate constants of the wild-type and M2 mutant AChRs are too fast to be reliably estimated, we used choline, a low-efficacy agonist that supports a slow opening rate constant (*14*). To isolate diliganded gating from the ligand-binding steps, the diliganded AChR opening rate constant (β) was estimated at a saturating concentration of agonist (20 mM choline). To relieve fast channel blockade by the agonist itself (which reduces the single-channel current amplitude and lengthens the apparent open channel lifetime), the diliganded AChR closing rate constant (α) was estimated at a low concentration of agonist (200 μM choline).

Segments of single-channel current traces were selected by eye, excluding noisy sections, long shut intervals, and segments containing openings of two or more overlapping channels. An interval-based full-likelihood algorithm, which includes a correction for missed events, was used to estimate rate constants [www.qub.buffalo.edu (*22*)]. The dead time was 25 or 62.5 μs (100 or 40 kHz sampling frequency, respectively), and the analysis bandwidth was between 4.5 and 10 kHz (10 kHz in most cases). The opening rate constant in the presence of choline is so slow that bursts of diliganded channel openings consist, mostly, of single openings. The reciprocal of the mean lifetime of these open intervals, measured at low ligand concentrations, is an overestimate of the (true) closing rate constant because, in addition to channel closure, agonist dissociation from the open state (followed by closure) and desensitization can also terminate an opening (*23*). The mean lifetime of diliganded AChR openings, in the presence of choline, can thus be approximated as the reciprocal of the sum of the closing rate constant, the choline dissociation rate constant from the open state, and the rate of entry into desensitization from the open state (*23*). For simplicity, the diliganded open state was modeled as having a single exit pathway, and the corresponding rate constant estimates were corrected by subtracting a value of 200 s^{-1}. This value is the slowest apparent closing rate constant that was observed (with the δL9′A construct), and therefore it is an upper limit for the sum of the desensitization and choline dissociation rate constants from the open state.

Linear Free Energy Relationships. The free energy change that the transition state of a two-state reaction experiences upon perturbation can be expressed, in some cases, as a linear combination of the free energy changes of the two end states (*15*). In the context of ion channel gating, this relation can be expressed as

$$(G^{\ddagger p} - G^{\ddagger}) = \Phi(G^{\circ p}_{open} - G^{\circ}_{open}) + (1 - \Phi)(G^{\circ p}_{closed} - G^{\circ}_{closed}) \quad (1)$$

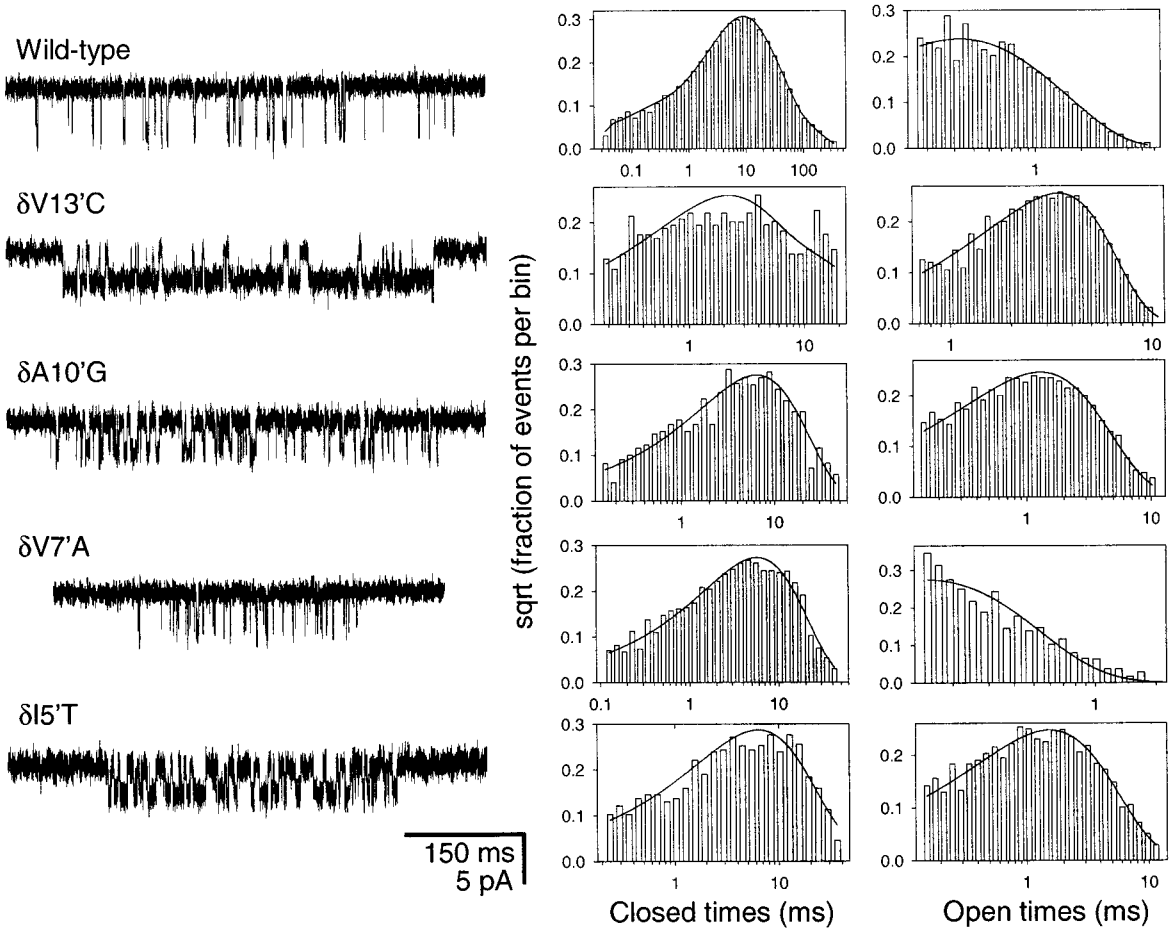

FIGURE 1: Single-channel kinetic analysis. (A, left) Example single-channel currents from the wild type and some of the δM2 mutants in the presence of 20 mM choline at a membrane potential of ~−100 mV. δM2 positions are numbered 1′−19′ from the intracellular to the extracellular end. For display purposes, the data were digitally filtered at 3 kHz. Openings are downward deflections. (B, right) Dwell time histograms and computed density functions. The closed time histograms correspond to currents elicited by 20 mM choline. The open time histograms correspond to currents elicited by 200 μM choline.

where ($G^{\ddagger p} - G^{\ddagger}$), ($G^{\circ p}_{open} - G^{\circ}_{open}$), and ($G^{\circ p}_{closed} - G^{\circ}_{closed}$) are the free energy changes upon perturbation (denoted by the superscript "p") experienced by the transition state, the open state, and the closed state, respectively, and Φ is a value between 0 and 1 that measures the position along the reaction coordinate of the mutated site at the transition state. A Φ-value of zero corresponds to a closed state-like structure, and a value of 1 corresponds to an open state-like structure. Thus, Φ is a measure of the extent to which the transition state resembles the open state, in the vicinity of the mutated residue. From eq 1, it follows that a double logarithmic plot of rate versus equilibrium constants (*18*) for a reaction series (i.e., the wild type plus a number of mutants at a given position) is a straight line, the slope of which is the parameter Φ

$$\log \beta = \Phi \log \beta/\alpha + \text{constant} \quad (2)$$

or (Φ − 1)

$$\log \alpha = (\Phi - 1) \log \beta/\alpha + \text{constant} \quad (3)$$

depending on the rate constant plotted on the *y*-axis (*15*).

RESULTS AND DISCUSSION

Linear Free Energy Relationships in δM2. The description of transition states is key to understanding mechanisms in single-step reactions. In this paper, we increased the spatial resolution of our previous characterization of the transition state of the AChR gating conformational change (*17*) by engineering series of mutations along the M2 domain of the mouse muscle δ subunit, estimating the corresponding opening and closing rate constants, and analyzing the results (rate and equilibrium constants) in the context of linear free energy relationships [LFERs (*15*, *16*)]. The M2 domain is a mostly α-helical transmembrane segment (*3*, *4*, *24*) oriented with its N-terminal end facing the cytoplasm and its C-terminal end facing the synaptic cleft (*2*). Its primary sequence, from the N-terminal to the C-terminal end, is

$$T^{1'}\mathbf{S}VA\mathbf{IS}V\mathbf{L}L^{9'}\mathbf{AQS}V\mathbf{F}LLL\mathbf{IS}^{19'}$$

Point mutations were engineered at positions 2′, 5′, 7′, 9′, 10′, 11′, 12′, 13′, 15′, 17′, and 19′ (in bold). The opening and closing rate constants of diliganded AChRs were estimated from single-channel patch-clamp recordings (Figure 1) using either saturating (for the opening rate constant) or low (for the closing rate constant) concentrations of choline, as detailed in Materials and Methods. Rate and equilibrium constants of diliganded gating were plotted as Brønsted relationships [log *k* versus log *K*; Figures 2 and 3 (*18*)], and the corresponding Φ-values were estimated as the slopes of linear fits (Table 1, and Figure 4).

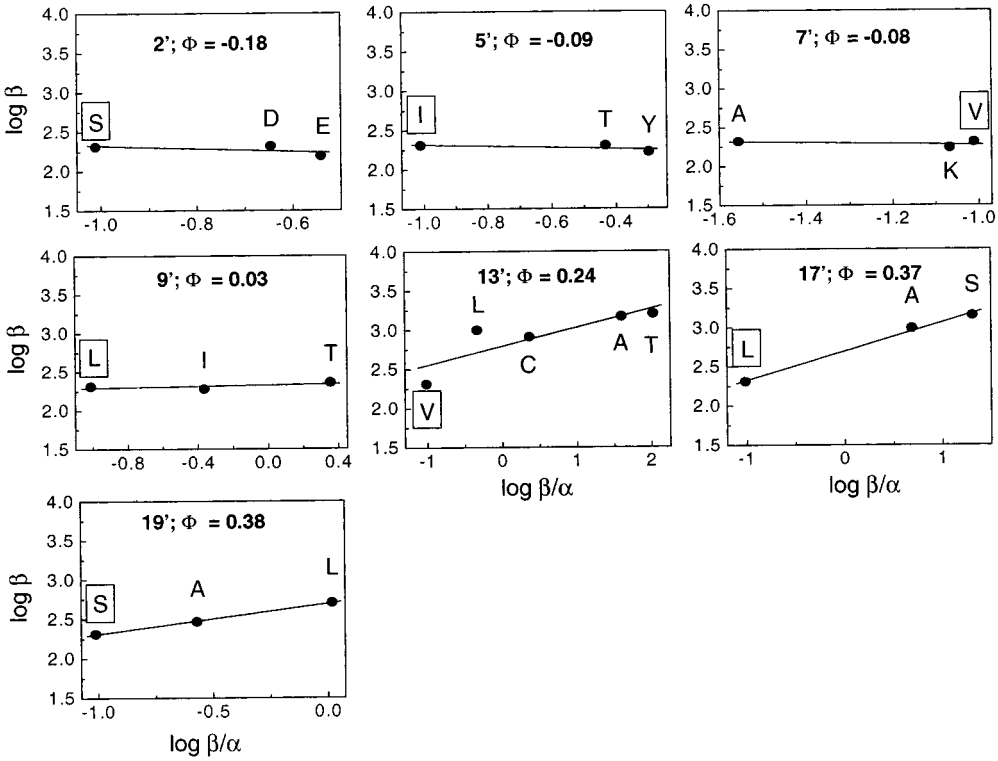

FIGURE 2: δM2 LFER analysis. Brønsted plots for most of the probed δM2 positions (denoted 1′−19′ from the intracellular to the extracellular end). Wild-type residues are enclosed by a rectangle. Φ-values are given by the slopes of linear fits to the plots. The 11′- and 15′-position data are omitted because, for technical reasons, their Φ-values could not be determined (see text). The Brønsted plot corresponding to the 10′-position is presented in Figure 3, and that corresponding to the 12′-position (*17*) is shown in Figure 6.

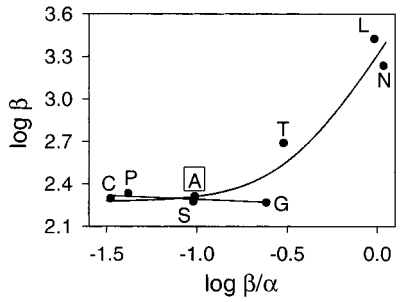

FIGURE 3: δM2 10′ LFER analysis. To account for the curvature of this plot, the data points were fitted with a model of two parallel transition states (curved line) using the equation $\log \beta = \log[\beta_{o1}(\beta/\alpha)^{\Phi_1} + \beta_{o2}(\beta/\alpha)^{\Phi_2}]$, where β_{o1} and β_{o2} are the diliganded receptor opening rate constants corresponding to the pathways that traverse either transition state when the equilibrium constant (β/α) is unity and Φ_1 and Φ_2 are the corresponding Φ-values at δM2 10′. Although this model fits the data better than a model of a single transition state (i.e., a fit to a straight line; not shown), the parameter estimates were ill-defined ($\beta_{o1} = 188 \pm 328$ s^{-1}; $\Phi_1 = 0 \pm 0.5$; $\beta_{o2} = 1835 \pm 625$ s^{-1}; $\Phi_2 = 2.1 \pm 1.3$), and the Φ-value of 2.1 is nonsensical in the context of an LFER. The slope of the straight line between the Ala (wild type; enclosed by a rectangle), Cys, Pro, Ser, and Gly constructs was −0.05 (excluding the Gly point from this fit changes this slope to −0.04). As another alternative, the wild-type's Φ-value at δ10′ was calculated as the first derivative of the curved line at the wild-type β/α value. This calculation yielded a value of 0.16, which does not affect the conclusions of this paper.

Table 1: Diliganded Gating Φ-Values at Different Positions along δM2

mutated residue[a]	Φ (mean ± SE)	equilibrium constant ratio[b]	no. of constructs[c]
S**2′**D,E	−0.18 ± 0.23[d]	3	3
I**5′**T,Y	−0.09 ± 0.10	5	3
V**7′**A,K	−0.08 ± 0.13	4	3
L**9′**A,T,I	0.03 ± 0.05[e]	23	4
A**10′**C,P,S,G,T,L,N	−0.05 ± 0.03[f]	33	8
Q**11′**A,S,L,T,K	ND[g]	ND	6
S**12′**A,G,W,C,T,I,Y,V,N,Q,K	0.28 ± 0.02[h]	1016	12
V**13′**A,C,L,T	0.24 ± 0.09	1090	5
L**15′**S,Q,P,F,N,E,Y	ND	ND	8
L**17′**A,S	0.37 ± 0.03	211	3
S**19′**A,L	0.38 ± 0.01	11	3

[a] Residues are numbered 1′−19′ from the intracellular to the extracellular end. [b] $\theta_{2\ \text{largest}}/\theta_{2\ \text{smallest}}$; diliganded gating equilibrium constants (θ_2) were calculated as the ratio between the diliganded opening (β) and closing (α) rate constants. [c] Including the wild type. [d] The large error estimate is likely to be due to the low equilibrium constant ratio obtained at this position. [e] The L9′A construct was not included when estimating the Φ-value for this position. The corresponding closing rate constant (α) was assumed to be unmeasurably low (see Materials and Methods). [f] Φ-value calculated considering the A (wild type), C, P, S, and G constructs. See text. For these constructs, the equilibrium constant ratio was 7. [g] Not determined. See text. [h] From ref *17*.

For residues below and including the 10′ position (2′, 5′, 7′, 9′, and 10′), Φ ranged between −0.18 and 0.03 (average Φ: −0.07). For residues above and including the 12′ position (12′, 13′, 17′, and 19′), Φ ranged between 0.24 and 0.38 (average Φ: 0.32). These values suggest that, when the transition state is reached, the gating reaction has proceeded to different extents in the upper and lower halves of δM2. The extracellular half resembles partly (∼30%) the open state, while the intracellular half is completely closed state-like.

The Brønsted plots were linear (Figure 2), with the exception of 10′ (Figure 3). This suggests that, at the mutated positions, the sensitivity of the transition state's free energy

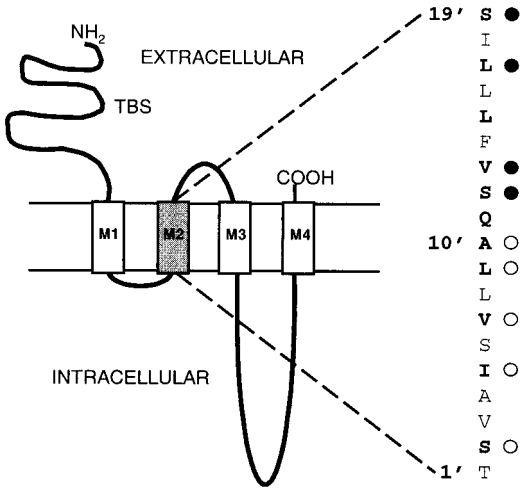

FIGURE 4: High-resolution map of Φ-values in δM2. Schematic representation of the AChR subunit topology. The transmitter binding sites (TBS) are ~45 Å away from the middle of the membrane (*6*, *12*, *13*). The channel pore is lined, for the most part, by the five M2 segments. Point mutations were engineered at positions indicated in bold. (○) Φ-value range, −0.18 to 0.03; (●) Φ-value range, 0.24 to 0.38. This pattern suggests that, during the opening reaction, the movement of the extracellular half of δM2 (12′ to 19′) precedes that of the intracellular half (2′ to 10′).

to mutations is a linear combination of the sensitivities of the closed and open states (eq 1). Insofar as energy and structure are related (*16*), this further suggests that the structure of M2 and its environment, at the gating transition state, is intermediate between the structures it adopts in the closed and open states (see Fractional Φ-Values, below).

General Observations. The effect of the mutations on gating (measured as the ratio between the largest and smallest equilibrium constant values in a given reaction series) was greatest in the extracellular half of M2 (Table 1). This suggests that the extracellular part of M2 undergoes a more pronounced change in environment between the closed and the open conformations. This observation is consistent with the results of cysteine-scanning mutagenesis in the $GABA_A$ receptor, which showed a greater tendency of disulfide bridge formation when Cys residues were engineered in the upper portion of M2 (*25*).

Another intriguing pattern was that, out of the 34 mutations that affected the diliganded gating equilibrium constant, 28 *increased* this value. Previous experiments (*14*) have shown that, at least in the M2 12′ position of the δ subunit, this increase in gating is due to an increased unliganded gating equilibrium constant (i.e., the intrinsic ability to gate) rather than to an increased affinity ratio (i.e., the ratio between the affinities of the ligand for the open and closed states), and it is reasonable to assume that the same is true for the other gain-of-function mutants in M2. On the other hand, three mutations near or at the ACh-binding sites were shown to *decrease* the unliganded gating equilibrium constant (*19*). Although the effect of more binding site mutations needs to be studied to make a firm generalization, it appears as though the primary sequences of the different domains of the wild-type AChR are differentially optimized with respect to unliganded gating.

Two out of the 11 probed δM2 positions (11′ and 15′) could not be assigned Φ-values. The changes in the gating equilibrium constant caused by mutations at the 11′ position (Gln → Ala, Gln → Ser, Gln → Leu, Gln → Thr, and Gln → Lys), were too small to be detected. This suggests that the structure of this portion of the δM2, or its nearest environment, changes little upon gating. Mutations at the 15′ position (Leu → Phe, Leu → Tyr, Leu → Ser, Leu → Gln, Leu → Glu, Leu → Pro, and Leu → Asn) either did not affect the gating equilibrium constant to a measurable extent or caused the gating kinetics to become heterogeneous in such a way that a single representative kinetic behavior could not be identified from the recordings.

The δM2 10′ Position. The Brønsted plot corresponding to the δM2 10′ position (Figure 3) was qualitatively different than the plots for other δM2 positions (Figure 2). While a linear plot indicates that the gross structure of the transition state is conserved despite the mutations, a curved Brønsted plot usually suggests a reaction that changes its mechanism as a function of the equilibrium constant (*15*). We therefore fitted the δ10′ Brønsted plot with a model of a reaction with two alternative transition states in *parallel* (Figure 3). Such a model predicts that the reaction mechanism switches from traversing one transition state at limiting low equilibrium constant values to traversing the other transition state at limiting large equilibrium constant values. At intermediate equilibrium constants, a mixture of both mechanisms occurs, the composition of which depends on the equilibrium constant of the reaction. Although the experimental points were fitted closely with this model, the parameter estimates were ill-defined and lacked physical significance: the Φ-value estimates of the two putative transition states, measured at the δ10′ position, were 0 ± 0.5 and 2.1 ± 1.3. Although a Φ-value of zero suggests a closed state-like environment for the δ10′ position at the transition state, a value larger than 1 cannot be attached any physical meaning in the framework of an LFER. Whether this lack of parameter definition and physical significance is simply due to the limited amount of data, or to the model of two parallel transition states being inappropriate, is not known.

A Φ-value larger than 1 cannot be interpreted easily. If the estimate of $\Phi = 2.1$ were accurate, all that could be said is that the change in free energy experienced by the transition state upon the Ala → Thr, Ala → Leu, and Ala → Asn mutations is not simply the linear combination of the corresponding changes experienced by the two ground states (i.e., the basic LFER premise; eq 1). That is, the transition state would be stabilized by these mutations to an extent that is larger than that expected solely as the result of the stabilization of the closed and open states. Although the data are limited, the δ10′ Brønsted plot suggests that such a "catalytic" effect would be more pronounced the more the energy landscape of gating is tilted toward the open state.

To estimate the Φ-value for the wild-type AChR at δM2 10′, we calculated the slope in the region of the plot where an LFER appears to hold, which are the points corresponding to the Ala (wild type) and the Cys, Pro, Ser, and Gly mutants. These constructs are well aligned, and the slope of a linear fit was −0.05. We conclude that, in the wild-type AChR, the δ10′ position has a Φ-value of approximately zero.

Two-Point LFERs. A thorough Φ-value analysis of a large protein with multiple different subunits, like the AChR, would require the detailed analysis of a very large number of mutants. Indeed, the complete Φ-value characterization of the AChR's gating reaction using Brønsted plots with,

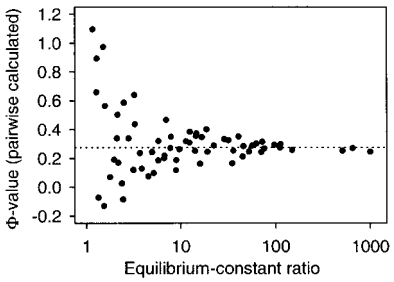

FIGURE 5: Effect of the ratio of equilibrium constants on the accuracy of Φ-values calculated from two-point LFERs. The data points corresponding to the wild type and 11 δ12′ mutants (*14*, *17*) were combined in all possible pairs (66 combinations). Φ-values were calculated for each pair using the corresponding rate and equilibrium constants and were plotted as a function of the respective ratios of equilibrium constants. The δ12′ data were used for this analysis because it is the most extensive LFER in our data. The horizontal dashed line is at $\Phi = 0.275$, the slope of the linear fit to the entire data set (*17*). As expected, the larger the ratio of equilibrium constants, the more accurate the pairwise estimate. The point corresponding to the Tyr-Val pair ($\Phi_{pairwise} = -1.82$; equilibrium constant ratio = 1.13) was omitted from the plot to allow a higher magnification scale.

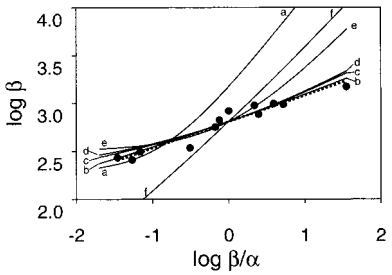

FIGURE 6: Rate equilibrium linear free energy relationships and physical interpretation of fractional Φ-values. The LFER data corresponding to the δ12′ mutant series were fitted with a straight line of slope (Φ) 0.275; this corresponds to a single transition state model (dotted line). The predictions of alternative models, consisting of either two [$\Phi_1 = 0$ and $\Phi_2 = 1$ (labeled as "a"); $\Phi_1 = 0$ and $\Phi_2 = 0.8$ ("e"); $\Phi_1 = 0.075$ and $\Phi_2 = 0.475$ ("d"); $\Phi_1 = 0.175$ and $\Phi_2 = 0.375$ ("b")] or 10 parallel transition states [equally spaced Φ-values between 0 and 0.55 ("c") and between 0.5 and 1 ("f")] were superimposed on the experimental points. Although the meaning of fractional Φ-values is not unambiguous, some interpretations can be ruled out. The predictions of the different models were calculated as $\log \beta = \log\sum_{i=1}^{k}\beta_{oi}(\beta/\alpha)^{\Phi_i}$, where β_{oi} is the diliganded receptor opening rate constant corresponding to the pathway that traverses transition state i when the equilibrium constant (β/α) is unity, Φ_i is the corresponding Φ-value, and k is the number of parallel transition states in the model. For the model of two competing transition states of $\Phi_1 = 0$ and $\Phi_2 = 1$ ("a"), the β_{oi} values were set so that the wild-type channel visits transition state 2 ($\Phi = 1$) 27.5% of the time and transition state 1 ($\Phi = 0$) the remaining 72.5% of the time (the probability of going through one or the other transition state is a function of the equilibrium constant in models with competing mechanisms). For the other models with multiple parallel transition states, the β_{oi}-values were arbitrarily considered to be identical, and equal to β_o/k, where β_o is the *observed* opening rate constant (i.e., due to all transition states) when $\beta/\alpha = 1$.

for example, four experimental points (the wild type plus three different mutant residues at any given position) would require the recording and analysis of single-channel data from ~5500 mutant receptors (~470 residues per subunit, four different subunits, three mutants per residue). To investigate how the accuracy of the Φ-value estimates would be affected if, instead, only one mutant per position were engineered (i.e., if two-point Brønsted plots were used), we calculated the Φ-values between all possible pairs of constructs for the δ12′ mutant series and plotted them as a function of the corresponding gating equilibrium constant ratios (Figure 5). This plot makes explicit a rather intuitive relationship, namely, that the slope of a linear function is more accurately estimated when the two experimental points are farther apart. This analysis suggests that, at least for this position, a ~10-fold change in equilibrium constant upon mutation is required for the error in a Φ-value, calculated from only two points, to be <0.1. We conclude that although drastic mutations can affect the protein to the extent that an LFER no longer holds (for example, Figure 3), mutations that are too mild (in the sense that they cause only small changes in the gating equilibrium constant) can lead to considerable errors in the estimation of Φ. The use of two-point Brønsted plots to estimate Φ values is the standard practice in studies exploring the transition state of protein folding (see refs *26* and *27*, for example), the field in life sciences that has been impacted the most, thus far, by the LFER approach.

Fractional Φ-Values. A Φ-value of zero (or 1) strongly suggests that the structure of the transition state near the mutated residue closely resembles the structure of the closed (or open) state. The interpretation of fractional Φ-values is, however, less straightforward (*28*). Two different interpretations have been put forward. According to one of them, a fractional Φ-value indicates the extent of a reaction at the time when the transition state is reached (*15*, *28*). Thus, the value of 0.24−0.38 estimated here for the extracellular part of δM2 would indicate that, at the transition state of gating, the structure of this region of the protein is 24−38% of what it is in the open and 62−76% of what it is in the closed state. Alternatively, it has been suggested that all the different trajectories linking the two end states might converge at two saddle points, one with $\Phi = 0$ and the other one with $\Phi = 1$ (*29*−*31*). In this framework, fractional Φ-values would reflect the probability of the channel traversing the free energy barrier through either transition state. According to this view, a value of, say, 0.3 would indicate that 30% of the openings (and 30% of the closings) occur via a transition state that is open-like ($\Phi = 1$) at the mutated site, whereas the remaining 70% of the barrier crossings occur via a transition state that is closed-like ($\Phi = 0$) in that region.

The occurrence of a Brønsted plot that is linear over a wide range of equilibrium constant values is compelling evidence in favor of the first interpretation, namely, that fractional Φ-values reflect an intermediate structure that is neither totally open (high ligand affinity and ion permeable) nor totally closed (low ligand affinity and ion impermeable). This argument, which has also been used to interpret fractional Φ-values in the context of protein folding (*28*, *32*), is elaborated here in Figure 6 for the case of AChR gating.

Single versus Parallel Transition States. A related question to that of the physical interpretation of fractional Φ-values is that of the number of transition states connecting the two end states. Linear Brønsted plots are interpreted as an indication of the existence of a single transition state (although not necessarily a single *pathway*) while curved plots can result from the existence of alternative, parallel transition states. As shown in the previous section and Figure 6, the curvature is predicted to be maximal when the Φ-values of the alternative transition states are 0 and 1.

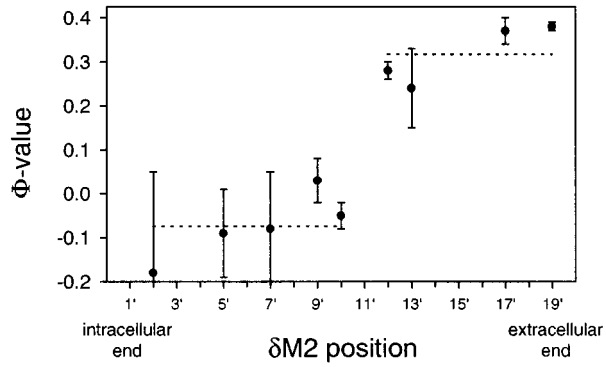

FIGURE 7: Φ-Values define two halves of δM2. There is an apparent clustering of Φ-values into two groups delimited by the middle of the δM2 transmembrane segment. The corresponding average Φ-values, indicated with horizontal dotted lines, are −0.07 (2′, 5′, 7′, 9′, and 10′; "the intracellular half") and 0.32 (12′, 13′, 17′, and 19′; "the extracellular half"). This discontinuity in the Φ-values near the midpoint of this mostly α-helical structure suggests that the rearrangement of the extracellular half precedes that of the intracellular half during opening (and follows during closing). Thus, we infer that the conformational changes associated with gating include the deformation of the backbone structure near the middle of δM2.

Because this curvature is predicted to decrease as the difference between these Φ-values gets smaller, we simulated a variety of models with parallel transition states and superimposed the predicted Brønsted plots on the experimental data points corresponding to the δ12′ mutant series. A cursory examination of the different plots suggests that the curvature predicted by a model of two alternative transition states of very different Φ-values (for example, 0 and 1 or 0 and 0.8) is inconsistent with the experimental data, as expected. On the other hand, a model of two transition states of very similar fractional Φ-values centered on 0.275 (e.g., 0.175 and 0.375) is practically indistinguishable from the straight line of slope 0.275, also as expected. Perhaps surprisingly, Figure 6 shows that a model with two transition states having Φ-values as different as 0.075 and 0.475, or a model consisting of 10 transition states in parallel with Φ-values equally spaced between 0 and 0.55 (i.e., centered on 0.275), describes the experimental points remarkably well. Thus, on the basis of the analysis in Figure 6, we cannot distinguish whether the reported Φ-values represent a property of a *single* transition state or an average property of an ensemble of transition states visited during gating.

Although this limitation of the LFER approach adds some ambiguity to the interpretation of our data, it does not compromise the conclusions. To emphasize this point, Figure 6 shows that a model consisting of 10 transition states in parallel, with Φ-values equally spaced between 0.5 and 1 (i.e., centered in 0.75), for example, would have not fitted our data. Thus, our decision of interpreting Φ-values as a property of a *single* transition state is, at least for the time being, based on parsimony.

Structural Implications. A simple interpretation of the pattern of Φ-values we obtained in δM2 (Table 1 and Figures 4 and 7) is that the two halves of this transmembrane segment move as distinct units during gating. On opening, the motion of the C-terminal (extracellular) part precedes that of the N-terminal (intracellular) portion while, on closing, the reverse mechanism takes place (*15*). These data, combined with our previous work (*14*, *17*), suggest that the different domains of the AChR attain the open state conformation in the following sequence: transmitter binding sites → M2−M3 loop → extracellular half of M2 → intracellular half of M2 (with the reverse sequence taking place during closing). This particular ordering of events indicates that the conformational change associated with opening does not reach M2 through the primary sequence (i.e., through the intervening M1 segment). If it did, then the intracellular half of M2 would be expected to be more open-like at the transition state (i.e., to have a higher Φ-value) than the extracellular half.

Several models of the conformational changes undergone by the M2 transmembrane segments during gating have been proposed. Although all of these models derive from experiments that probed very different properties of the M2 domain, they all converge to the idea that this transmembrane segment does not move as a rigid body during gating. Using cryoelectron microscopy, Unwin (*7*, *33*) described the existence of a kink, near the midpoint of M2, that changes during gating in a manner that is consistent with its being a swiveling or bending point. Using the substituted cysteine accessibility method, Karlin and Akabas (*8*) proposed the transition from an extended structure (in the closed state) to an α-helical structure (in the open state) at the level of the 8′−10′ residues of M2. We note that this short nonhelical segment would afford a higher flexibility to this part of M2, perhaps allowing the formation of a molecular hinge. Using unnatural amino acid mutagenesis, England et al. (*34*) found that amide-to-ester backbone mutations in the 8′−10′ M2 region affect the channel's function in a way that is consistent with the secondary structure of this part of M2 changing during gating. Also, using molecular dynamics simulations of a pentameric helix bundle of M2 segments embedded in a phospholipid bilayer, Law et al. (*9*) added further evidence for this proposed backbone rearrangement in the vicinity of the central 9′ Leu. Our observation of a discontinuity of Φ-values around the 10′ position (Figures 4 and 7), derived from analyzing the correlation between rate and equilibrium constants of mutant series in δM2, strongly supports this general concept. That is, δM2 does not move as a rigid body during the closed ⇌ open reaction. Further, as discussed above, our results suggest a temporal order for the rearrangement of the two halves of δM2 during gating. The LFER approach, however, does not provide any information as to the magnitude of the motion about the midpoint of δM2.

In contrast with structural models of gating that posit conserved α-helical structures above and below the 8′−10′ region (*7*−*9*, *33*), the results of England et al. (*34*) suggest that the backbone deformation in the upper half of αM2 (13′, 16′, and 19′ positions) is *larger* than that in the middle of M2. All of these models would be consistent if the backbone conformational changes above 8′−10′ did not introduce additional kinks, did not alter the α-helical pattern of solvent accessibility, and did not affect the rigidity of the extracellular half of M2 observed in the molecular dynamics simulations. Moreover, our results using an LFER approach are also not inconsistent with a model invoking extensive backbone rearrangements during gating (*34*). Rather, our data add new insight as they suggest that changes in secondary structure undergone by the different residues in the extracellular half of δM2 must take place almost synchronously, all being ∼30% complete when the transition state is reached.

However, at that same point in time, the conformational changes in the intracellular half of M2 (backbone or otherwise) would have not yet started (Figure 7).

The existence of a flexure point, within an otherwise well-ordered secondary structure, may be needed to lower the free energy of the transition state in order for AChR gating to meet the physiological requirements of fast synaptic transmission. The 9′ and 10′ positions are well conserved in the superfamily of pentameric ligand-gated ion channels, and thus, it is likely that other neurotransmitter-gated ion channels also have flexible pore-lining segments that optimize their function. Interestingly, a flexure point near the middle of a transmembrane α-helix has been suggested to play a crucial role in the function of the light-driven ion pump bacteriorhodopsin (*35*, *36*). Application of the LFER methodology to other ion channels is needed to determine whether the bending of a pore-lining α-helix is a common feature of the mechanism of gating.

ACKNOWLEDGMENT

We thank Raquel Lima, Timothy Bailey, and Mary Teeling for technical assistance in molecular biology and cell culture.

REFERENCES

1. Imoto, K., Methfessel, C., Sakmann, B., Mishina, M, Mori, Y., Konno, T., Fukuda, K., Kurasaki, M., Bujo, H., and Fujita, Y. (1986) *Nature 324*, 670−674.
2. Imoto, K., Busch, C., Sakmann, B., Mishina, M., Konno, T., Nakai, J., Bujo, H., Mori, Y., Fukuda, K., and Numa, S. (1988) *Nature 335*, 645−648.
3. White, B. H., and Cohen, J. B. (1992) *J. Biol. Chem. 267*, 15770−15783.
4. Akabas, M. H., Kaufmann, C., Archdeacon, P., and Karlin, A. (1994) *Neuron 13*, 919−927.
5. Zhang, H., and Karlin, A. (1998) *Biochemistry 37*, 7952−7964.
6. Unwin, N. (1993) *J. Mol. Biol. 229*, 1101−1124.
7. Unwin, N. (1995) *Nature 373*, 37−43.
8. Karlin, A., and Akabas, M. H. (1995) *Neuron 15*, 1231−1244.
9. Law, R. J., Forrest, L. R., Ranatunga, K. M., La Rocca, P., Tieleman, D. P., and Sansom, M. S. P. (2000) *Proteins 39*, 47−55.
10. Tikhonov, D. B., and Zhorov, B. S. (1998) *Biophys. J. 74*, 242−255.
11. Pashkov, V. S., Maslennikov, I. V., Tchikin, L. D., Efremov, R. G., Ivanov, V. T., and Arseniev, A. S. (1999) *FEBS Lett. 457*, 117−121.
12. Herz, J. M., Johnson, D. A., and Taylor, P. (1989) *J. Biol. Chem. 264*, 12439−12448.
13. Valenzuela, C. F., Weign, P., Yguerabide, J., and Johnson, D. A. (1994) *Biophys. J. 66*, 674−682.
14. Grosman, C., and Auerbach, A. (2000) *J. Gen. Physiol. 115*, 637−651.
15. Leffler, J. E., and Grunwald, E. (1963) in *Rates and Equilibria of Organic Reactions*, Wiley, New York.
16. Fersht, A. R., Matouschek, A., and Serrano, L. (1992) *J. Mol. Biol. 224*, 771−782.
17. Grosman, C., Zhou, M., and Auerbach, A. (2000) *Nature 403*, 773−776.
18. Brønsted, J. N., and Pedersen, K. (1924) *Z. Phys. Chem. 108*, 185−235.
19. Grosman, C., and Auerbach, A. (2000) *J. Gen. Physiol. 115*, 621−635.
20. Salamone, F. N., Zhou, M., and Auerbach, A. (1999) *J. Physiol. 516*, 315−330.
21. Hamill, O. P., Marty, A., Neher, E., Sakmann, B., and Sigworth, F. J. (1981) *Pfluegers Arch. 391*, 85−100.
22. Qin, F., Auerbach, A., and Sachs, F. (1996) *Biophys. J. 70*, 264−280.
23. Grosman, C., and Auerbach, A. (2001) *Proc. Natl. Acad. Sci. U.S.A. 98*, 14102−14107.
24. Le Novère, N., Corringer, P.-J., and Changeux, J.-P. (1999) *Biophys. J. 76*, 2329−2345.
25. Horenstein, J., Wagner, D. A., Czajkowski, C., and Akabas, M. H. (2001) *Nat. Neurosci. 4*, 477−485.
26. Itzhaki, L. S., Otzen, D. E., and Fersht, A. R. (1995) *J. Mol. Biol. 254*, 260−288.
27. McCallister, E. L., Alm, E., and Baker, D. (2000) *Nat. Struct. Biol. 7*, 669−673.
28. Fersht, A. R., Itzhaki, L. S., ElMasry, N. F., Matthews, J. M., and Otzen, D. E. (1994) *Proc. Natl. Acad. Sci. U.S.A. 91*, 10426−10429.
29. Straub, J. E., and Karplus, M. (1990) *Protein Eng. 3*, 673−675.
30. Sali, A., Shakhnovich, E., and Karplus, M. (1994) *J. Mol. Biol. 235*, 1614−1636.
31. Onuchic, J. N., Socci, N. D., Luthey-Schulten, Z., and Wolynes, P. G. (1996) *Folding Des. 1*, 441−450.
32. Kim, D. E., Yi, Q., Gladwin, S. T., Goldberg, J. T., and Baker, D. (1998) *J. Mol. Biol. 284*, 807−815.
33. Unwin, N. (2000) *Philos. Trans. R. Soc. London, Ser. B 355*, 1813−1829.
34. England, P. M., Zhang, Y., Dougherty, D. A., and Lester, H. A. (1999) *Cell 96*, 89−98.
35. Subramaniam, S., and Henderson, R. (2000) *Nature 406*, 653−657.
36. Royant, A., Edman, K., Ursby, T., Pebay-Peyroula, E., Landau, E. M., and Neutze, R. (2000) *Nature 406*, 645−648.

BI011864F